

Enhanced Magnetic Resolution in Elliptical Planar Hall Effect Sensors via Non-Collinear Anisotropy Engineering

Daniel Lahav¹, Moty Schultz¹, Asaf Grosz² and Lior Klein¹

¹Department of Physics, Institute of Nanotechnology and Advanced Materials, Bar-Ilan University, Ramat-Gan 52900, Israel

²Department of Electrical and Computer Engineering, Ben-Gurion University of the Negev, P.O. Box 653, Beer-Sheva 84105, Israel

Introduction

Elliptical planar Hall effect (EPHE) sensors operate by coherent magnetization rotation, so their sensitivity and equivalent magnetic noise (EMN) are set by the effective anisotropy field H_{eff} . Conventionally the growth (H_g) and shape (H_s) anisotropies are collinear and add, $H_{\text{eff}} = H_s + H_g$, fixing a floor $H_{\text{eff}} \geq H_g$. We pattern the ellipse orthogonal to the growth easy axis, so the contributions compensate, $H_{\text{eff}} = |H_s - H_g|$, reaching the $H_{\text{eff}} < H_g$ regime. Across three geometry pairs this lowered H_{eff} (e.g. 6.15 to 2.66 Oe), matching a parameter-free model within 0.2 Oe while preserving few-pT/VHz/A operation.

Fundamentals & Working Principle

Effective Anisotropy from Mixed Uniaxial Contributions

When several in-plane uniaxial contributions coexist, the total anisotropy energy density can be written as

$$E_{\text{ani}}(\theta) = \sum_i K_i \sin^2(\theta - \phi_i)$$

Two-Term Reduction

$$E_{\text{ani}}(\theta) = E_0 + K_{\text{eff}} \sin^2(\theta - \phi_{\text{eff}})$$

$$K_{\text{eff}} = \sqrt{K_1^2 + 2K_1K_2 \cos 2\phi_2 + K_2^2} \quad \phi_{\text{eff}} = \frac{1}{2} \arctan 2(K_2 \sin 2\phi_2, K_1 + K_2 \cos 2\phi_2)$$

Orthogonal Shape-Growth Configuration

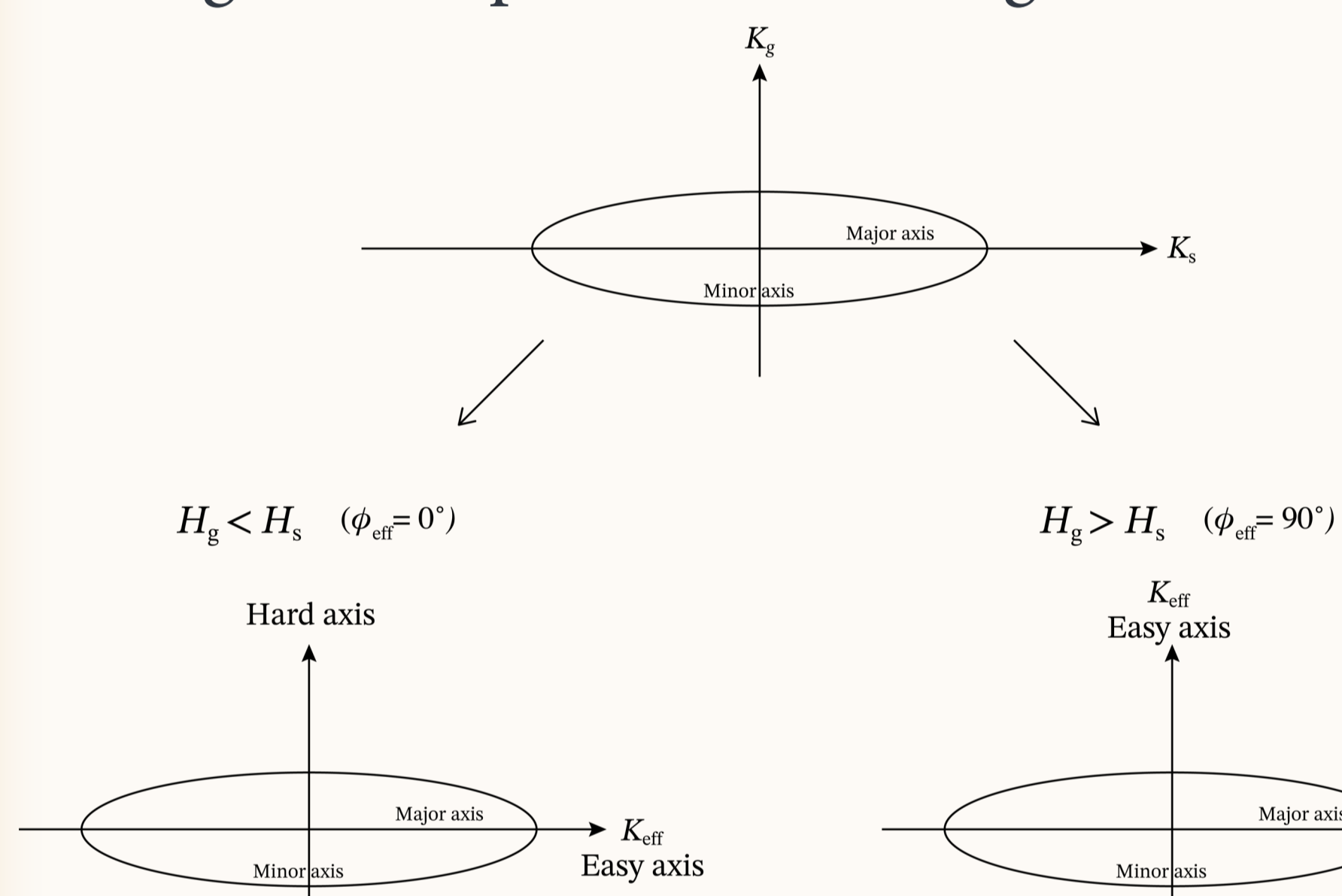


Fig. 2. Schematic of orthogonal mixing in an EPHE sensor between the shape anisotropy H_s , defined by the ellipse major axis, and the growth-induced anisotropy H_g . In the orthogonal configuration, the two contributions partially compensate, yielding $H_{\text{eff}} = |H_s - H_g|$. The effective easy-axis direction is set by the dominant contribution.

Magnetoresistance

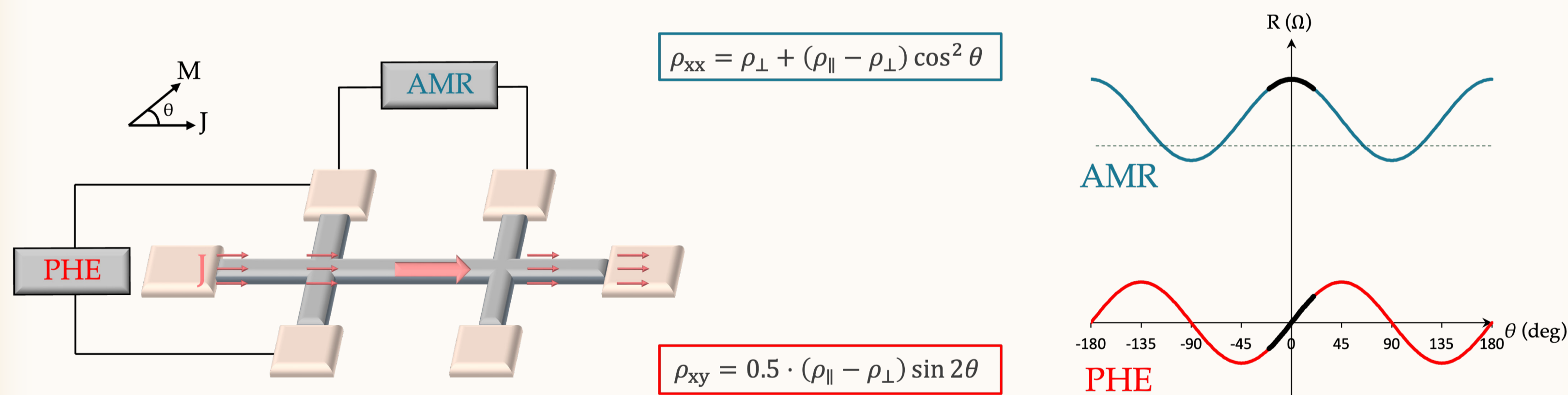


Fig. 3. Typical Hall-cross pattern used to measure AMR and PHE, with the dependence of the longitudinal and transverse resistance on the angle θ between the current J and the magnetization M . The longitudinal resistance follows $\cos^2 \theta$ (AMR, blue), while the transverse resistance follows $\sin 2\theta$ (PHE, red).

Elliptical Planar Hall Effect Sensors

The elliptical shape of PHE sensors induces uniaxial 'shape anisotropy' along the long axis. For a flat ellipsoid with thickness t , major axis a , and minor axis b , the anisotropy field is: $H_s \sim 4\pi M_s \frac{t}{b}$

Sensitivity

The sensitivity (S_y) of a PHE sensor is the ratio of its PHE voltage (V_y) to the applied magnetic field in the y -direction (H_y), for a given current (I_x) along the easy axis.

$$S_y = \frac{V_y}{H_y} = I_x \frac{\Delta \rho}{t} \frac{1}{H_s + H_g} = I_x \frac{\Delta \rho}{t} \frac{1}{H_{\text{eff}}}$$

Excitation current I_x , Sensor thickness t , Growth-induced anisotropy H_g , Resistivity anisotropy $\Delta \rho = (\rho_{\parallel} - \rho_{\perp})$, Shape anisotropy H_s .

Equivalent Magnetic Noise (EMN)

$$\text{EMN}(f) = \frac{e_{\Sigma}(f)}{S_y}$$

The total noise spectral density (e_{Σ}) has three main components: $1/f$ noise, thermal noise (both originating from the sensor), and preamplifier noise. Namely:

$$e_{\Sigma}(f) = \sqrt{e_{1/f}^2 + e_T^2 + e_{\text{amp}}^2}$$

$1/f$ noise dominates at low frequencies, while thermal (white) noise prevails at high frequencies.

Design and Materials

Permalloy (Py, Ni₈₀Fe₂₀) is used as the ferromagnetic sensing layer for its high PHE sensitivity and low coercive field. Tantalum (Ta) serves as a capping layer that protects the Py from oxidation and environmental degradation.

A schematic of the sensor showing the major (a) and minor (b) axes of the ellipse and the gold contact pads (yellow).

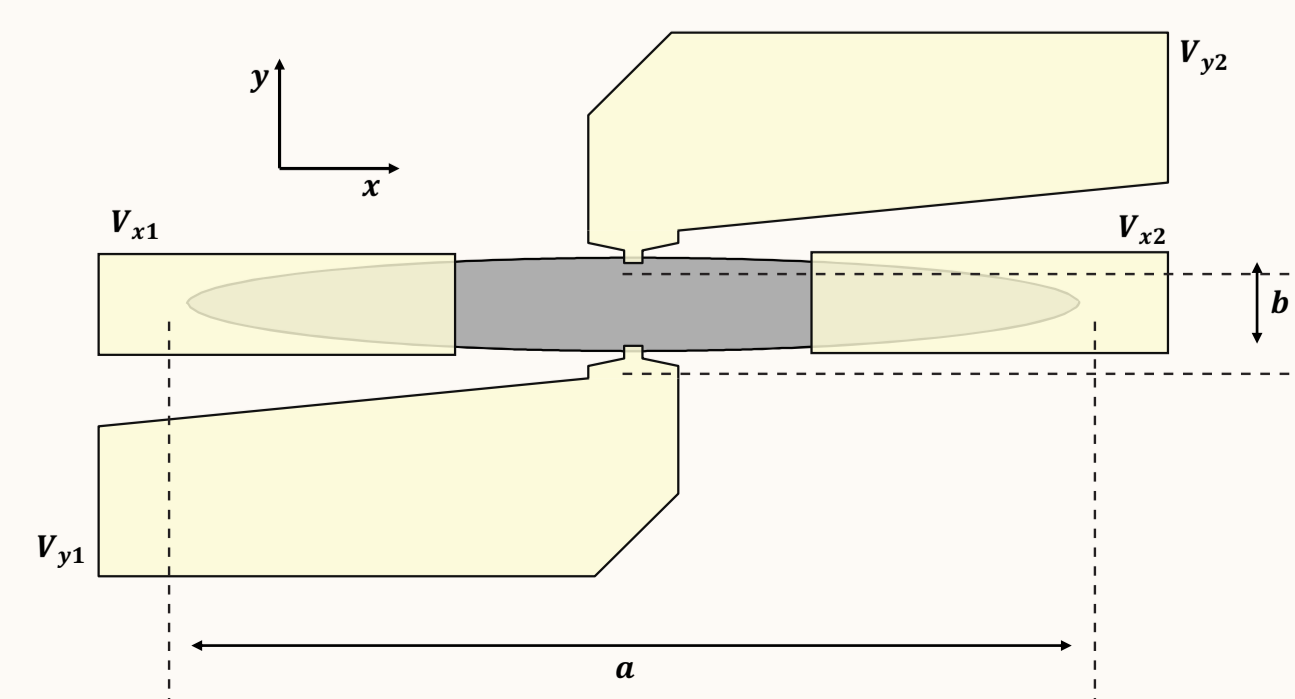


Fig. 4. Schematic of an elliptical PHE sensor.

The sensor is excited with an ac current between V_{x1} and V_{x2} , and the signal is measured at V_{y1} and V_{y2} .

Results

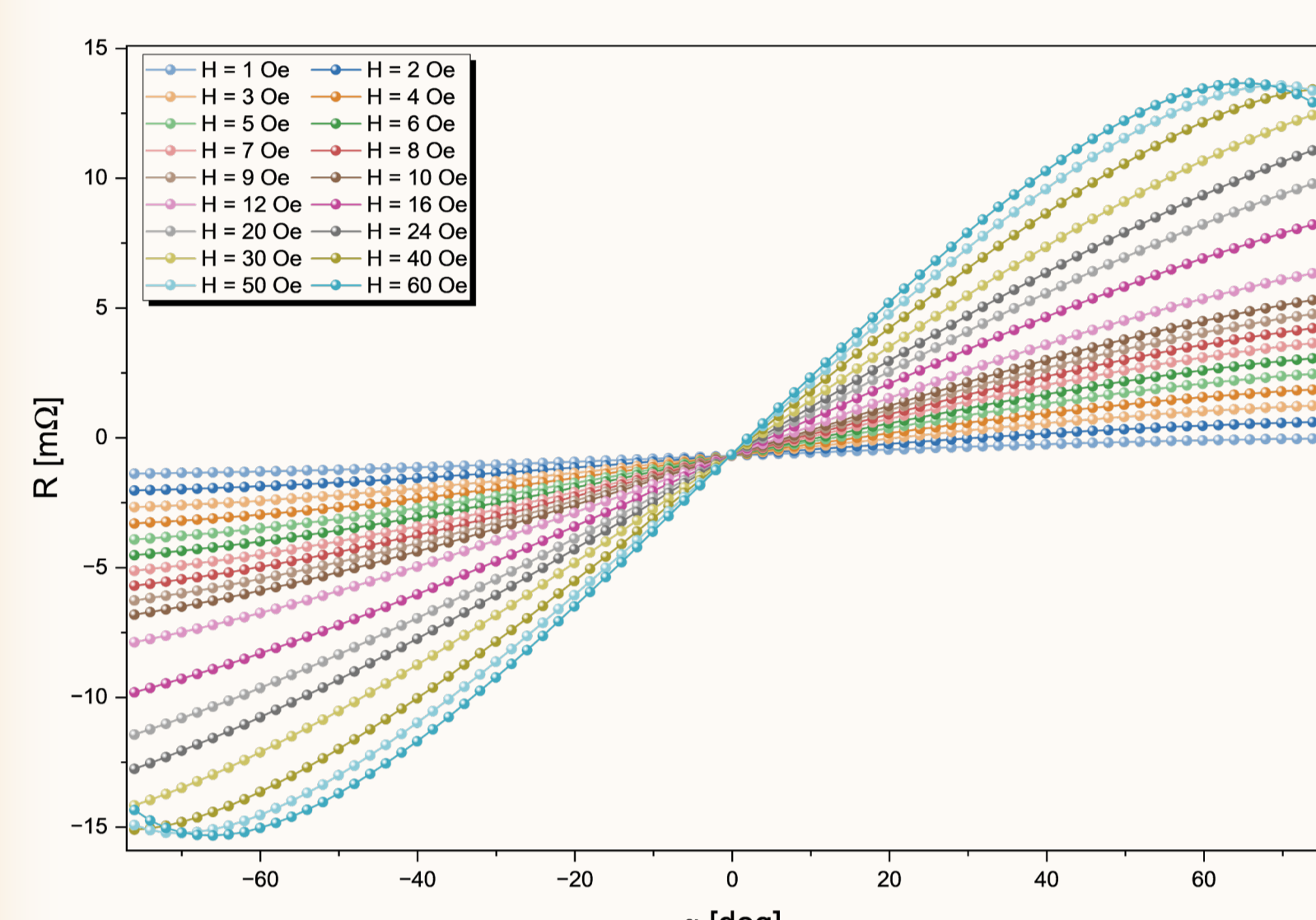


Fig. 5. Representative angular resistance sweeps $R(\alpha)$ measured under multiple fixed in-plane magnetic fields. The field-dependent evolution of the angular response provides the dataset used for the torque-balance-based extraction of the effective anisotropy parameters.

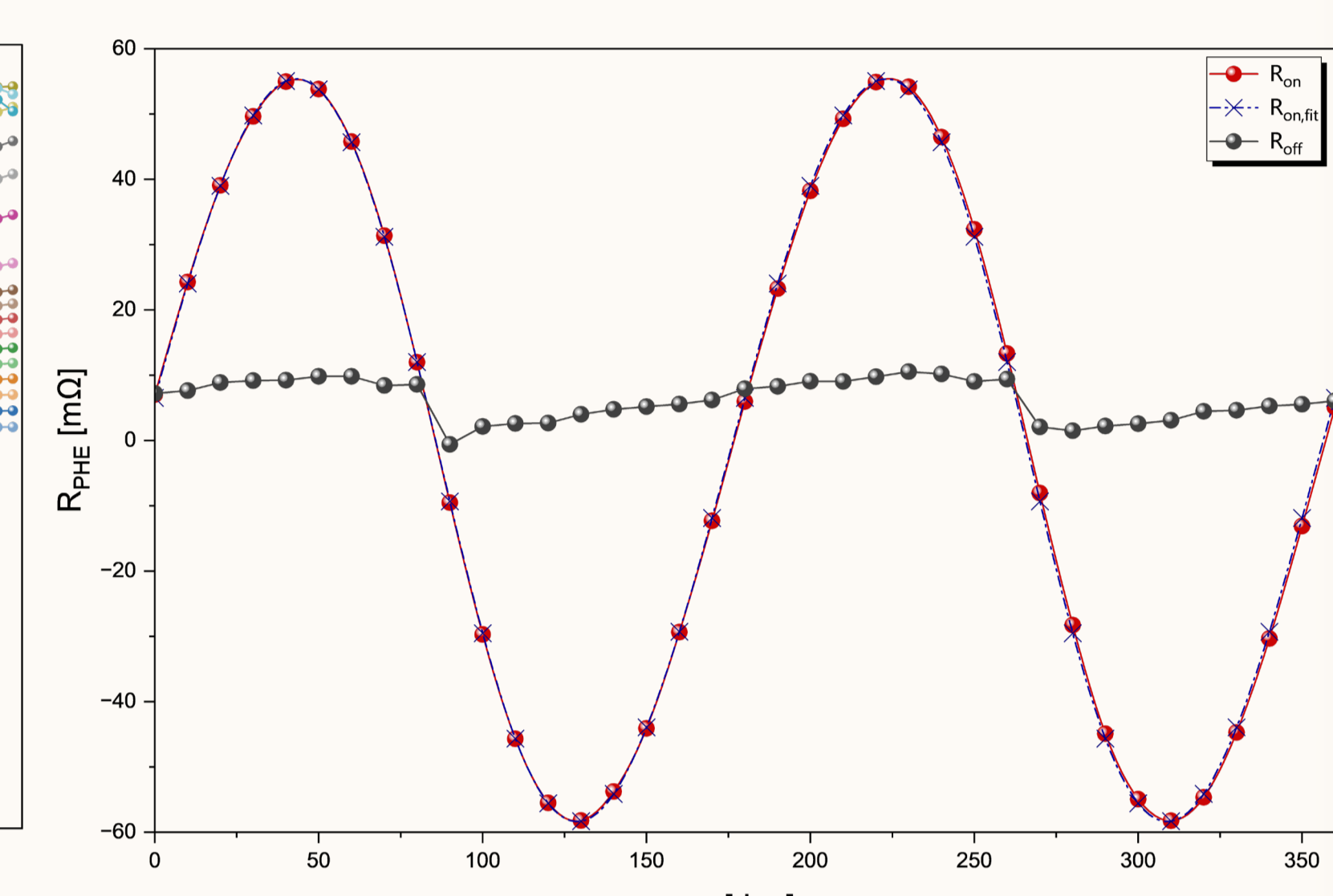


Fig. 6. Representative field-varying PHE measurement analyzed via the torque-balance condition, with the corresponding fit. This analysis provides an independent consistency check of the extracted H_{eff} and ϕ_{eff} .

t (nm)	b (μm)	H_s^{asym} (Oe)	H_s^{Osb} (Oe)	H_g (Oe)	H_{eff} (Oe)	$H_{\text{eff}}^{\text{std}}$ (Oe)	$H_{\text{eff}}^{\text{model}}$ (Oe)	ϕ_s (deg)	ΔR_{PHE} (m Ω)
50	625	0.86	0.81	4.28	5.14	0.02	5.14	0	114.6
50	625	0.86	0.81	4.28	3.60	0.11	3.42	90	115.7
50	400	1.35	1.28	4.39	5.74	0.09	5.74	0	104.8
50	400	1.35	1.28	4.39	2.93	0.13	3.04	90	110.1
100	625	1.73	1.64	4.42	6.15	0.06	6.15	0	58.8
100	625	1.73	1.64	4.42	2.66	0.17	2.69	90	57.9

Table 1. Summary of extracted anisotropy and electrical parameters for the studied EPHE devices. H_s^{asym} is the calculated shape-anisotropy field from the asymptotic form, H_s^{Osb} is the corresponding Osborn evaluation, H_{eff} is the effective anisotropy field extracted from the SW fit, $H_{\text{eff}}^{\text{std}}$ is the corresponding fit uncertainty, and $H_{\text{eff}}^{\text{model}}$ is the expected value from the limiting mixing rules. H_g is back-extracted from the corresponding $\phi_s = 0^\circ$ device of the same pair using the asymptotic H_s .

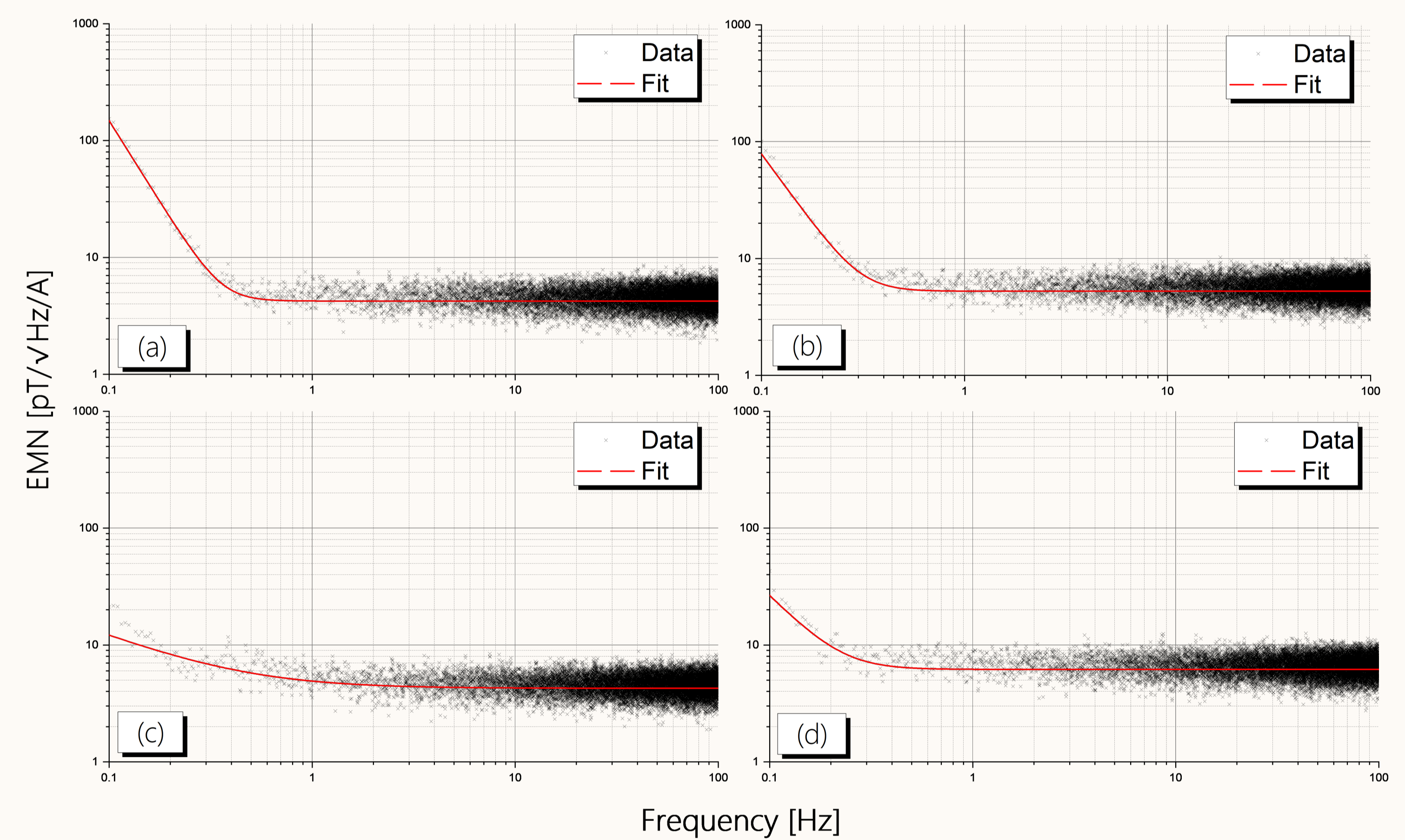


Fig. 7. Representative current-normalized EMN spectra of the four $t = 50$ nm EPHE devices: (a) $b = 625 \mu\text{m}$, $\phi_s = 0^\circ$; (b) $b = 625 \mu\text{m}$, $\phi_s = 90^\circ$; (c) $b = 400 \mu\text{m}$, $\phi_s = 0^\circ$; and (d) $b = 400 \mu\text{m}$, $\phi_s = 90^\circ$. Crosses: measured data; solid red line: fit to the low-frequency-plus-white-noise form.

t (nm)	b (μm)	ϕ_s (deg)	H_{eff} (Oe)	Norm. sens. (V/T/A)	EMN (pT/ $\sqrt{\text{Hz}}$ /A)		
					@1 Hz	@10 Hz	@100 Hz
50	625	0	5.14	208.2	4.24	4.23	4.23
50	625	90	3.60	170.6	5.26	5.25	5.25
50	400	0	5.74	148.8	6.20	6.18	6.18
50	400	90	2.93	216.2	4.91	4.29	4.26
100	625	0	6.15	119.7	6.57	6.44	6.44
100	625	90	2.66	175.8	4.63	4.62	4.62

Table 2. Normalized sensitivity and current-normalized EMN values for the full studied device set. The four $t = 50$ nm devices are shown in Fig. 7; the $t = 100$ nm, $b = 625 \mu\text{m}$ pair is included here for completeness.

Conclusions

- Orienting the ellipse major axis orthogonal to the growth easy axis makes the shape and growth anisotropies partially compensate, giving $H_{\text{eff}} = |H_s - H_g|$ and access to the $H_{\text{eff}} < H_g$ regime that the collinear scheme ($H_{\text{eff}} = H_s + H_g$) cannot reach.
- Across three matched geometry pairs, switching from parallel to orthogonal lowered H_{eff} in every case (e.g. 6.15 \rightarrow 2.66 Oe), matching a parameter-free mixing model to within 0.2 Oe.
- Back-extracted growth anisotropy collapsed to $\langle H_g \rangle = 4.36 \pm 0.07$ Oe across separate growth runs, confirming both the reproducibility of the deposition recipe and the precision of the device-level model.
- The devices stayed in the few-pT/VHz/A current-normalized EMN range, so anisotropy-orientation control is a footprint-preserving lithographic knob for low-anisotropy, high-resolution EPHE sensors.

Scan For More

